ARTICLES

^{1}H MAS and ^{1}H/^{27}Al TRAPDOR NMR Studies of Oxygen−Zeolite Interactions at Low Temperatures: Probing Bronsted Acid Site Accessibility

Haiming Liu, Hsien-Ming Kao, and Clare P. Grey*

Chemistry Department, State University of New York at Stony Brook, Stony Brook, New York 11794-3400

Received: September 11, 1998; In Final Form: March 30, 1999

Sorption of oxygen in the pores of zeolite HY and ^{1}H MAS NMR has been used to determine which Brønsted acid sites are accessible to oxygen. Large increases in the ^{1}H spinning-sideband manifolds are observed at low temperatures for the supercage protons that can directly interact with the oxygen molecules; a much smaller increase in sideband intensity is seen for the sodalite protons. Dramatic reductions of the T_1's of all the protons, of approximately 2 orders of magnitude, are observed at −150 °C, in comparison to T_1 measurements made in air at room temperature, or at −150 °C for samples with adsorbed N_2. The T_1's of the supercage protons are, however, shorter than those measured for the sodalite protons. Both the decrease in the T_1's, and the large sideband manifolds, are due to the dipolar coupling interactions with the unpaired electrons present on the O_2 molecules. Second moment (M_2) analysis is used to quantify the increase in the width of the ^{1}H spinning sideband manifolds, in samples of zeolites HY and HZSM-5. Comparison between samples run in air and with fixed loading levels of oxygen allows changes in loading level with temperature to be detected and oxygen loading levels to be estimated. The contribution to M_2 of the protons due to bulk magnetic susceptibility effects and from oxygen molecules that do not directly interact with the protons was estimated from the values of M_2 extracted from the ^{29}Si MAS NMR of the same samples. The contribution to M_2 from the direct interaction of the protons with the oxygen molecules could then be estimated.

Introduction

Paramagnetic ions have been widely exploited in solution NMR spectroscopy[1−3] to increase resolution or sensitivity, by exploiting their shift or relaxation properties. There are now a number of studies of paramagnetic compounds in the solid state, the study of these materials becoming progressively more feasible, with the development of probes that allow MAS NMR experiments to be performed at increasingly fast MAS spinning frequencies.[4−7] The relaxation effect on nearby nuclear spins has been exploited in solid state NMR, particularly for low sensitivity $I = {}^1/_2$ nuclei in materials where the spin lattice relaxation times (T_1's) of the spins would otherwise be very long (e.g., ^{29}Si NMR of silicates). The reduction of the ^{29}Si T_1's of porous materials such as zeolites, from minutes to ∼ 0.2−2 s, in the presence of paramagnetic oxygen molecules is well established,[8] the decrease in the T_1's resulting from the interaction between the nuclear (^{29}Si) and electronic moments due to the two unpaired electrons in the two degenerate highest occupied π^* orbitals of O_2. More recently, O_2 has been used as a shift reagent to probe accessibility of cations and protons in zeolites.[9−11] We published a short communication in which we demonstrated that O_2 can be used to discriminate between protons in the supercages and sodalite cages of zeolite HY:[9] shorter T_1's and large spinning sideband manifolds were observed for protons in the supercages that are in direct contact with the O_2. In an earlier report, Zscherpel et al.[12] showed that oxygen broadens the ^{1}H MAS NMR spinning sideband pattern of the protons in HZSM-5 loaded with oxygen, especially at low temperatures. The Brønsted acid sites were no longer detected at coverages higher than 1 O_2 molecule per unit cell (uc) at low temperatures, presumably because the width of the spinning sideband pattern becomes extremely large. The second moment of the ^{1}H MAS NMR signal was found to be closely related to the temperature and the oxygen loading, lower temperatures and higher loading levels leading to larger second moments. In a recent report,[10] the combination of oxygen sorption and ^{6}Li MAS NMR was shown to be an effective method for determining the cations accessible to O_2: Shifts were observed for resonances assigned to the SIII cations in the supercages of lithium LSX. We observed much larger shifts in the ^{133}Cs MAS NMR resonances of cations in the supercages of Y and X zeolites.[9,13] We ascribed these shifts to a Fermi-contact mechanism, caused by the formation of short-lived Cs^+−O_2 complexes.

In this paper, we report results from a more extensive ^{1}H MAS NMR study of Brønsted acid and silanol protons in HY and HZSM-5. In particular, we have studied the ^{1}H−O_2 interactions at low temperatures to explore whether MAS NMR can be used to probe O_2 sorption and binding and the size of cage or channel openings in zeolites. An analysis of the second moments of the ^{1}H resonances in these samples is presented. ^{1}H/^{27}Al TRAPDOR (transfer of populations in double resonance) NMR[14] was used to separate the Brønsted acid sites and silanol groups in HZSM-5. The ^{1}H/^{27}Al TRAPDOR NMR method allows aluminum species, such as Brønsted and Lewis acid sites, and aluminum hydroxides, to be studied via the

10.1021/jp983686e CCC: $18.00
Published on Web 05/19/1999

(dipolar) coupling to nearby aluminum atoms. TRAPDOR NMR makes use of the passages that occur between the Zeeman levels of the quadrupolar nucleus (^{27}Al), under conditions of slow MAS and continuous irradiation, to alter the evolution of a proton coupled to an ^{27}Al spin, following an initial ^{1}H $\pi/2$ pulse. Magic angle spinning results in a time dependence of the (^{27}Al) quadrupolar interaction, and the quadrupole splitting sweeps through zero two or four times per rotor period (the "zero crossings"), for each individual spin in the powdered sample, depending on the relative orientation of the quadrupole and rotor principal axis systems. These crossings result in population transfers between the six ^{27}Al Zeeman levels. The population transfers then prevent refocusing of the dipolar coupled ^{1}H spins at the ^{1}H spin−echo experiment, causing a TRAPDOR effect. The TRAPDOR fraction, defined as the reduction of the (^{1}H) echo signal intensity with respect to that obtained without ^{27}Al irradiation, will depend on the dipolar coupling between spins: the greater the dipolar coupling, the greater the TRAPDOR effect. Further details of this experiment may be found in earlier references.[14,15]

It may sometimes be difficult to analyze a system with many interactions, and possibly with many motions. One traditional method for extracting the size of an interaction, and the effect of motion on the spin system, is to use second moment analysis.[16] Under MAS conditions, the second moment M_2 may be determined by measuring the amplitudes (or areas) of the spinning sidebands belonging to a particular resonance in the frequency-domain spectrum and is experimentally defined by[16]

$$M_2 = \omega_r^2 \Sigma k^2 (A_k/\Sigma A_k) \quad (1)$$

where ω_r is the spinning speed, k is the order of a sideband, and A_k is the amplitude of the kth sideband. In the case of the ^{1}H MAS NMR spectra of HY and HZSM-5, spinning sidebands are mainly caused by three interactions: (i) the heteronuclear dipolar interaction with the neighboring aluminum nucleus (Brønsted acid protons), (ii) the homonuclear dipolar interaction between protons, and (iii) the chemical shift interaction.[17,18] Therefore, the sideband envelope contains information concerning the homonuclear and heteronuclear dipolar interactions, and chemical shift anisotropy (CSA), which may be extracted by analyzing the second moment of the spinning sideband pattern:

$$M_2 = M_2^{HAl} + M_2^{HH} + M_2^{CSA} \quad (2)$$

where M_2^{HAl} is the second moment of the H−Al dipolar interaction, M_2^{HH} is that of the H−H interaction, and M_2^{CSA} is the second moment due to the CSA. If oxygen is present, the interaction between the O_2 unpaired electrons and the proton spins contributes to the width of the spinning sideband manifolds as well. $M_2^{en'}$, the experimentally measured change in total second moment (M_2), due to this dipolar interaction, may be extracted from the following expression:

$$M_2^{en'} = M_2 - (M_2^{HAl} + M_2^{HH} + M_2^{CSA}) \quad (2a)$$

Second moment analyses are, therefore, used to follow changes in the magnitude of the O_2−^{1}H interactions in HY and HZSM-5 at various temperatures.

Experimental Section

Sample Preparation. HZSM-5 and HY were prepared under shallow-bed conditions by deammoniation of NH_4ZSM-5 (Si/Al = 25) and NH_4Y (Si/Al = 2.6), respectively. The ammonium forms were first evacuated at room temperature, dehydrated at 120 °C for 12 h and then slowly heated to 400 °C at a rate of 12 °C /h. The temperature was maintained at 400 °C for a further 24 h. The dehydrated samples were packed into Kel-F inserts in a glovebox under an inert N_2 atmosphere. The inserts, which help prevent rehydration, are not completely airtight and do not prevent O_2/N_2 from entering the sample. The samples were kept in sealed vials until immediately before the experiments. In order to load oxygen into the samples, dehydrated HZSM-5 samples were packed into a specially designed 3.4 mm Pyrex tubes in a glovebox. The Pyrex samples tubes were then attached to the vacuum line and defined amounts of oxygen were trapped in the tubes. The tubes were cooled in liquid nitrogen and then flame-sealed to give small capsules that could be used for the MAS experiments. Two HZSM-5 samples with loading levels of 1 and 4 O_2/uc were prepared. Zirconia rotors were used to spin samples contained in either Kel-F inserts or glass capsules.

NMR Experiments. Variable temperature ^{1}H MAS and ^{1}H/^{27}Al TRAPDOR NMR experiments were performed with a double-tuned Chemagnetics 5 mm probe on a CMX-360 spectrometer. Experiments were also run with a Chemagnetics 5 mm double resonance probe, on a CMX-200 spectrometer, to explore the effect of the field strength on the second moment. Liquid nitrogen boil-off gas was used as the heater gas and, for some experiments, also as the spinning gas (bearing and drive) in place of compressed air. The heater and spinning gases are essentially isolated in the Chemagnetics variable temperature design. Exchange between the spinning gas (bearing) and gas inside the rotor occurs, unless samples are sealed in glass ampules. Thus samples acquired with air as the bearing (and drive) gases, in Kel-F inserts, are exposed to air. A 90°−τ−180°−τ−(acquire) spin−echo sequence was used to acquire all the ^{1}H MAS spectra to remove the broad proton background signal due to the probe. An evolution time and refocusing time (τ) of one rotor period was used throughout. Additional ^{1}H single pulse spectra (not shown) were also acquired to ensure that no resonances were lost in the spin−echo spectra. An inversion−recovery pulse sequence was used for ^{1}H T_1 measurements. Spinning rates of 4.00 kHz and recycle delays of 2 s were used throughout unless denoted. ^{1}H chemical shifts are quoted relative to TMS.

An ^{27}Al radio frequency field strength of 60 kHz was used for the ^{1}H/^{27}Al TRAPDOR experiment. The TRAPDOR experiment consists of two experiments. In the first, the control experiment, a rotor synchronized ^{1}H spin−echo experiment is performed. In the second, the double resonance ^{1}H/^{27}Al TRAPDOR experiment, ^{27}Al irradiation is applied during the evolution period (τ) of the ^{1}H spin−echo experiment. Again, τ = 1 rotor period. A difference spectrum is obtained by subtracting the TRAPDOR spectrum from the control spectrum. Further details of this experiment can be found elsewhere.[14]

^{29}Si MAS NMR spectra were acquired at an operating frequency of 71.52 MHz, on the higher field NMR instrument, with recycle delays of 10 s and $\pi/6$ pulses of 2 μs. Spectra were referenced to TMS, at 0 ppm.

Results

Figure 1 shows the effect of temperature on the ^{1}H MAS NMR spectra of dehydrated HY. As the temperature is decreased, the spinning sideband manifolds of the two major resonances gradually increase, and by −150 °C, a dramatic increase in the spinning sideband manifolds is observed for samples run in dry air (i.e., in the air used for sample spinning). In contrast, when N_2 is used, very little difference is observed between the room and low-temperature spectra. On close

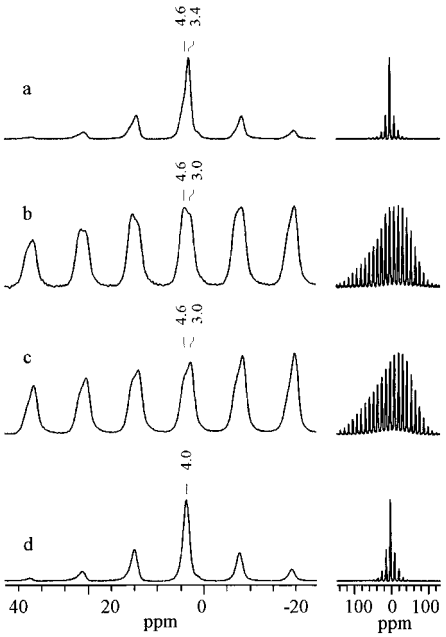

Figure 1. The ^{1}H MAS NMR spectra of HY acquired (a) at room temperature in air, and at −150 °C in air with (b) a pulse delay of 2 s, (c) a pulse delay of 0.01 s, and (d) at −150 °C under an N_2 atmosphere. The full spectra are shown on the right. Spectra were acquired at 360 MHz (^{1}H Larmor frequency) with a spinning rate of 4.0 kHz.

inspection, two distinct sets of spinning sideband manifolds are observed in air at low temperatures. One sideband manifold contains spinning sidebands that cover more than 260 ppm (94 kHz) and an isotropic resonance of 3.0 ppm. The resonance has shifted by 0.4 ppm from the room temperature (25 °C) value of 3.4 ppm and is assigned, on the basis of the chemical shift, to protons in the supercages of the faujasite structure.[19] The second spinning-sideband manifold, with an associated isotropic resonance of 4.6 ppm, is considerably narrower covering about 160 ppm (58 kHz). This resonance is assigned to protons in the sodalite cages.[19] The intensity of each spinning sideband was extracted, by deconvolution of the individual sidebands, and then plotted against its shift (Figure 2). The large sideband manifold assigned to protons in the supercages and the narrower one ascribed to those in the sodalite cages can now be clearly distinguished. A ratio of 1:0.52 between the total intensities of the two types of Brønsted acid sites is obtained (supercage: sodalite cage protons), close to the value of 1:0.57 at room temperature. The second moments of the protons in sodalite cages and supercages, calculated from the intensities of the individual sidebands by using eq 1, are 7.7×10^8 and 6.3×10^8 s^{-2}, respectively, at room temperature, similar to the results of Hunger et al.[18] At −150 °C, drastically increased values of 34×10^8 and 120×10^8 s^{-2}, respectively, are obtained. The second moment of the sodalite cage protons is considerably smaller than that of the supercage protons, corresponding to the narrower sideband manifold. When a 0.01 s recycle delay is used, a decrease in the intensity of the resonance from the sodalite-cage protons is seen, in comparison to the intensity observed in the spectrum acquired with the usual 2 s recycle delay. This indicates that the sodalite protons have a longer T_1 at this temperature, in comparison to that of the supercage protons. Large differences in T_1 are measured for the protons in air at different temperatures and are about 0.4 s for both protons at room temperature and 0.006 and 0.012 s for the supercage and sodalite protons, respectively, at −150 °C (Table 1). The two resonances could be separated by acquiring two spectra, one with long and one with short recycle delays, and

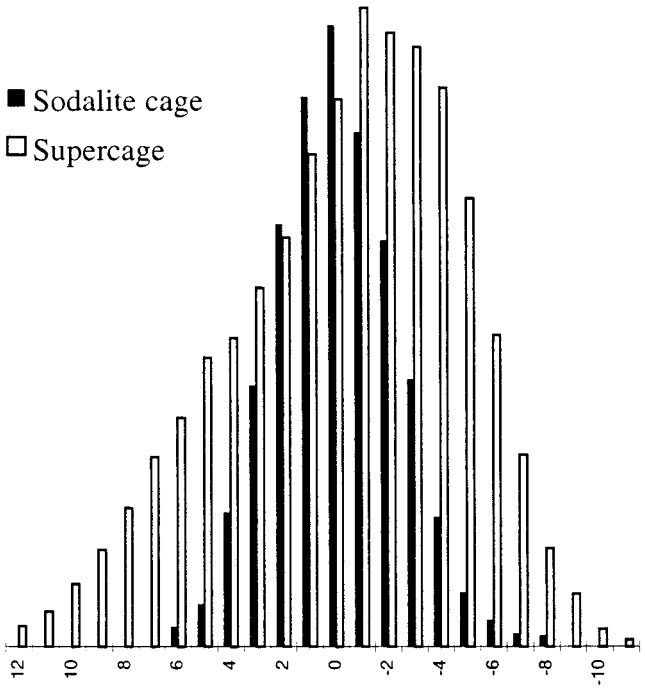

Figure 2. The two sideband manifolds due to the Brønsted acid sites in the (solid bars) sodalite cages and those in the (open bars) sodalite cages, obtained by deconvolution of the ^{1}H MAS NMR spectra of HY acquired at −150 °C in air with a pulse delay of 2 s. The order of the spinning sidebands is marked on the *x* axis.

TABLE 1: ^{1}H T_1 (in seconds) for Dehydrated HY and HZSM-5 in Air

	HY		HZSM-5		
	H_B (sodalite)[a]	H_B (supercage)	H_B at 4.0 ppm	H_B at 7 ppm	silanol proton
room temperature	0.39	0.38	0.22	0.23	0.36
−150 °C	0.006	0.012	0.008	0.009	0.014

[a] H_B = Brønsted acid proton.

subtracting the one spectrum from the other (not shown). It should be noted that a longer T_1 of 1.7 s is measured for the Brønsted acid protons in N_2, at −150 °C.

Variable temperature ^{1}H MAS NMR spectra of HZSM-5 in air show a similar temperature-dependent behavior (Figure 3). ^{1}H/^{27}Al TRAPDOR NMR is used to separate the Brønsted acid sites and silanol groups in HZSM-5, because only the latter is seen, at 2.0 ppm, in the experiment performed with ^{27}Al irradiation (Figure 4). Difference spectra are obtained by subtracting the ^{1}H/^{27}Al TRAPDOR NMR spectra from the corresponding ^{1}H MAS NMR spin−echo spectra (Figure 5). Only protons in the vicinity of ^{27}Al, i.e., the Brønsted acid sites in this case, are seen in the difference spectra. In addition to the resonance from the Brønsted acid sites at 4.0 ppm, a broad resonance at 7 ppm, with associated sidebands, is clearly visible in the TRAPDOR difference spectrum. This indicates that it results from protons with short H−Al internuclear distances that are similar to the H−Al distances of the Brønsted acid site at 4.0 ppm (≈2.48 Å[20,21]). A TRAPDOR fraction of 94% was obtained for the 7.0 ppm resonance. This large TRAPDOR effect and the width of the sideband manifolds are in agreement with the previous assignment of the 7 ppm resonance to a second Brønsted acid site: This broad resonance was first noted by Brunner et al.[22] at about 7 ppm in the ^{1}H MAS NMR spectra of HZSM-5 acquired at 123 K and was assigned to bridging hydroxyls (Brønsted acid sites) that are shifted from the normal chemical shift position for Brønsted acid sites, due to an

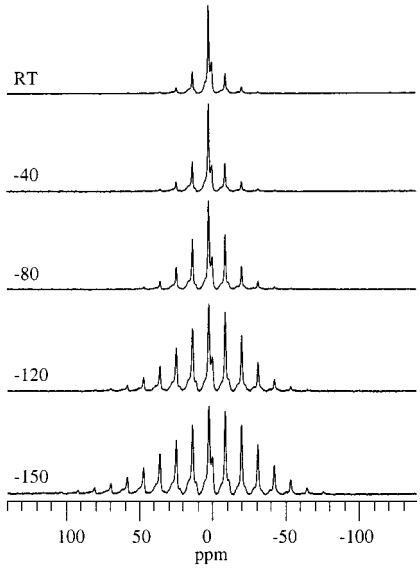

Figure 3. The ^{1}H MAS NMR spectra of HZSM-5 at various temperatures in air.

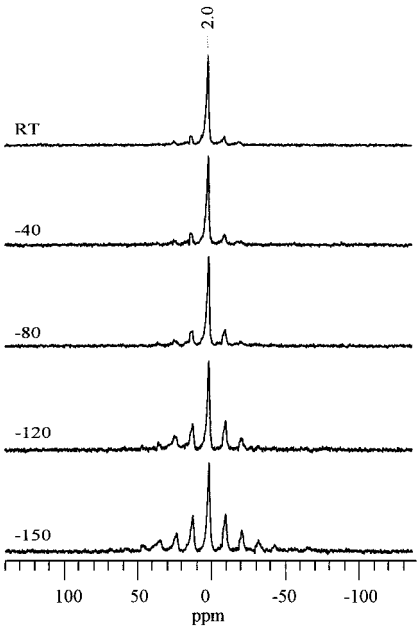

Figure 4. The ^{1}H/^{27}Al TRAPDOR NMR spectra of HZSM-5 at various temperatures in air acquired with ^{27}Al irradiation.

additional H-bond interaction with the zeolite framework. Beck et al.[23] also independently observed this resonance (at 6.9 ppm) in HZSM-5 at low temperatures and ascribed it to a second Brønsted acid site on the basis of double-resonance ^{1}H{^{27}Al} and 2D exchange experiments. Later Freude,[24] using heteronuclear dipolar-dephasing spin−echo (or TRAPDOR) MAS NMR, concluded that the proton at this site can jump between two or more of the four oxygen atoms around a central aluminum atom, and at one of these positions, is affected by an additional electrostatic interaction with another framework oxygen atom. The line width of the resonance at 7 ppm, obtained in our experiments, is larger than that of the Brønsted acid site at 4.0 ppm, suggesting that there is a distribution of the local environments for the second Brønsted acid site. Unlike in HY, the two types of acidic protons in HZSM-5 have similar sideband manifold widths at all temperatures. There is a noticeable change in the shape of the sideband manifolds with

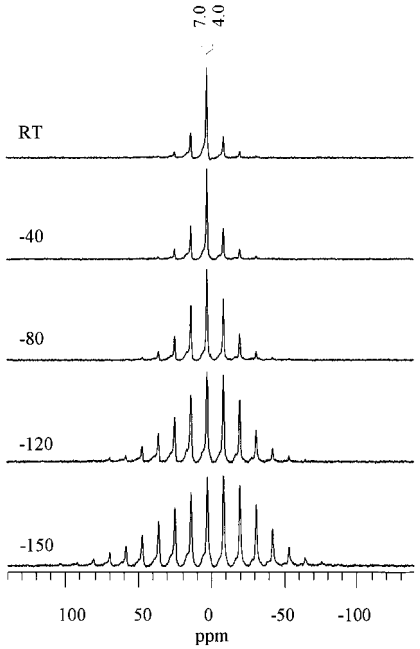

Figure 5. The difference spectra at various temperatures obtained by subtracting the ^{1}H/^{27}Al TRAPDOR NMR spectra from the corresponding ^{1}H MAS NMR echo spectra.

temperature, the asymmetry increasing significantly at low temperatures: At 25 °C, the first low-frequency spinning sideband of the Brønsted acid site at 4.0 ppm is less intense than the high-frequency one. With decreasing temperature, however, the intensity of the former grows more rapidly than that of the latter and at temperatures below −80 °C is larger than that of the high-frequency one. The second moments of the Brønsted acid sites at 4.0 and 7 ppm were extracted, by deconvoluting the difference spectra. These grow rapidly from 5.7×10^8 and 5.6×10^8 s^{-2} at 25 °C to 54×10^8 and 77×10^8 s^{-2}, respectively, at −150 °C. An enhancement in the width of the sideband manifolds is also observed at low temperatures for the silanol protons, but the effect is much smaller (Figure 4). The second moment of the silanol protons, extracted from the ^{1}H/^{27}Al TRAPDOR NMR spectra, increases from about 0.5×10^8 s^{-2} at 25 °C to 18×10^8 s^{-2} at −150 °C. A reduction in the T_1 from 0.22 s at 25 °C to 0.008 s at −150 °C is measured for the 4.0 ppm Brønsted acid sites. The T_1 of the resonance at 7 ppm, with a value of 0.009 s at −150 °C, is only slightly longer than the T_1 of the resonance at 4.0 ppm. A decrease in T_1, from 0.36 to 0.014 s, is also observed for the silanol groups between the room and low-temperature measurements (Table 1).

Experiments were repeated for HZSM-5 at a field strength corresponding to a ^{1}H frequency of 200 MHz. Again the spinning sideband intensities increase as the temperature is lowered but not as dramatically as was observed at higher fields. The 7 and 4 ppm resonances could not be so well resolved and thus separate M_2 values could not be obtained for the individual resonances. Average M_2 values were, therefore, obtained by integration of the 4/7 ppm sidebands (in the difference spectrum). The spectra acquired in air and in N_2 are similar at room temperature.

The acidic protons and the silanol protons are rigid at room temperature,[25] and thus the second moments due to H−Al, H−H dipolar interactions, and CSA are assumed to remain constant as the temperature decreases. The spectra acquired in N_2 are consistent with this assumption, as little change is noticed between the spectra at room and low temperatures. The increase

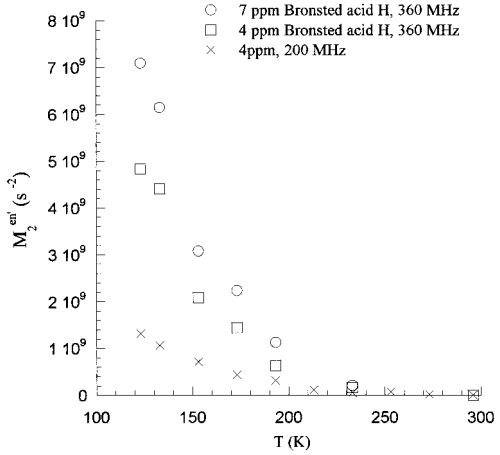

Figure 6. The increase in the second moment due to the interaction between O_2 and the Brønsted acid sites, $M_2^{en'}$, for the resonances at (open circles) 7 ppm and at (open squares) 4.0 ppm in HZSM-5, at a ^{1}H Larmor frequency of 360 MHz, and at (crosses) 4.0 ppm at 200 MHz, as a function of temperature.

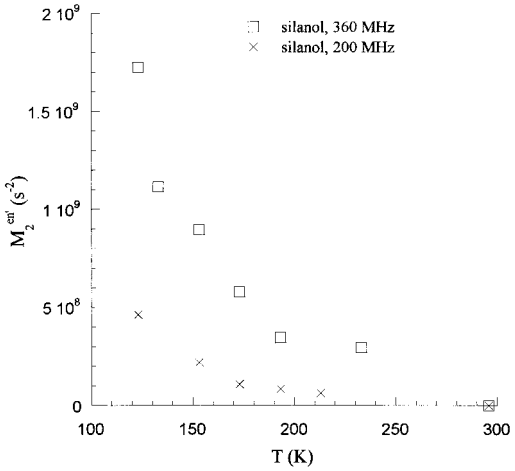

Figure 7. The increase in the second moment due to the interaction between O_2 and the silanol groups in HZSM-5 at (open squares) 360 MHz and (crosses) 200 MHz as a function of temperature.

in the second moment due to the O_2-^1H interaction, $M_2^{en'}$, of the acidic protons and the silanol protons were, therefore, extracted by subtraction of the second moment at 25 °C from those at lower temperatures, for the two series of data acquired at 360 and 200 MHz. $M_2^{en'}$ of the acidic protons is plotted as a function of the absolute temperature (Figure 6). Figure 7 shows a similar plot obtained for the silanol groups. As expected, a higher magnetic field and lower temperatures lead to larger values of $M_2^{en'}$.

Two HZSM-5 samples loaded with fixed amounts of oxygen (1 and 4 O_2/uc) were examined, to allow comparison with samples run in air. Figure 8 shows the variable temperature ^{1}H/^{27}Al TRAPDOR NMR spectra of HZSM-5 loaded with 1 O_2/uc acquired (a) without or (b) with ^{27}Al irradiation. The difference spectra are shown in (c). A new, sharp resonance appeared at 6.3 ppm at 25 °C due to the adsorption of small amount of water, presumably introduced during the oxygen loading process. This resonance has been previously ascribed to water molecules bound to the Lewis acid sites.[26] Lewis acid sites in HZSM-5 may be generated during dehydration and deammoniation, especially at temperatures above 400 °C. This resonance was also observed in the TRAPDOR difference spectra, and was associated with a TRAPDOR fraction of about 40%, consistent with recent results of Deng et al.[27] The Brønsted

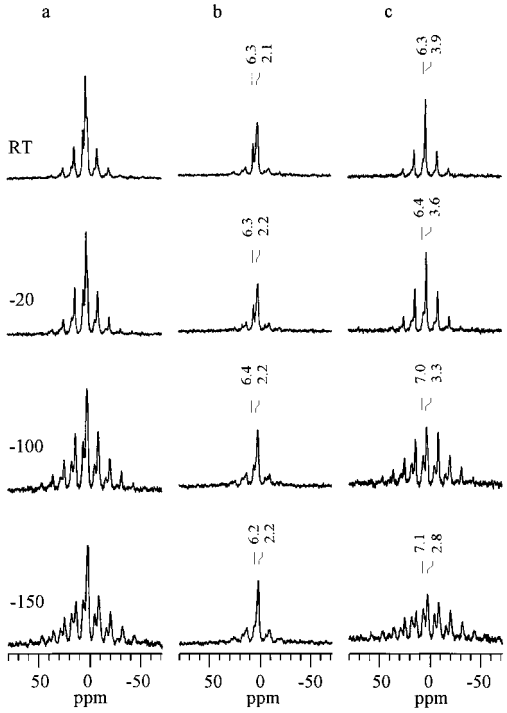

Figure 8. The variable temperature ^{1}H/^{27}Al TRAPDOR NMR spectra of HZSM-5 loaded with 1 O_2/uc acquired (a) with and (b) without ^{27}Al irradiation. The difference spectra are shown in (c). Temperatures (°C) are marked on the spectra.

acid resonance, at 3.9 ppm at room temperature, shifts to lower frequency with decreasing temperature, and is located at 3.6, 3.3, and 2.8 ppm at −20, −100, and −150 °C, respectively. At lower temperatures, the resonance overlaps with the silanol peak, but it can be clearly resolved in the difference spectrum. The width of the sideband manifold also increases, but the increase is not as large as that for the sample spun with dry air. At temperatures below −100 °C, the asymmetry of the spinning sideband pattern is reversed, as was observed for the sample in air. A significant decrease in the signal-to-noise ratio is also observed. No shift is observed for the silanol resonance, but again, there is a small increase in sideband intensity, as seen in the TRAPDOR spectra. The sharp resonance at 6.3 ppm gradually broadens and shifts in the opposite direction, reaching 7.1 ppm at −150 °C. The width of its sideband manifold is greatly enhanced. Furthermore, the TRAPDOR fraction of this resonance increases to about 80%, suggesting a stronger H−Al dipolar interaction for the protons associated with this resonance. This may be due to a decrease in the mobility of the water molecules. This will lead to a larger H−Al dipolar coupling and, therefore, a larger TRAPDOR fraction, and also larger spinning sideband manifolds, due to increased H−H dipolar interactions. Alternatively, the second Brønsted acid site, which has a large TRAPDOR effect, may also be contained under the larger spinning sideband manifolds. This resonance would also be expected to shift slightly to lower frequencies at lower temperatures, as was observed for the 4 ppm Brønsted acid site, but because of its larger line width it may not be so clearly seen. At 25 °C, the T_1's of the Brønsted acid sites, the water at the Lewis-acid sites and the silanols are much shorter than those measured for the protons in HZSM-5 in air (Table 2). The T_1's of the Brønsted acid protons measured at −60 °C and at −150 °C are very similar (0.007 s).

An HZSM-5 sample loaded with 4 O_2/uc was studied by ^{1}H/^{27}Al TRAPDOR NMR at five different temperatures: 25, −20, −60, −100, and −150 °C. Spectra collected (a) with, (b) without

TABLE 2: ^{1}H T_1 (in seconds) for HZSM-5 Samples Loaded with Oxygen

	1 O_2/uc			4 O_2/uc		
	4 ppm	6.3 ppm	Silanol	3.1 ppm	6.3 ppm	Silanol
room temperature	0.02	0.04	0.07	0.009	0.01	0.03
−20 °C				0.006		
−60 °C	0.007					
−150 °C	0.007					

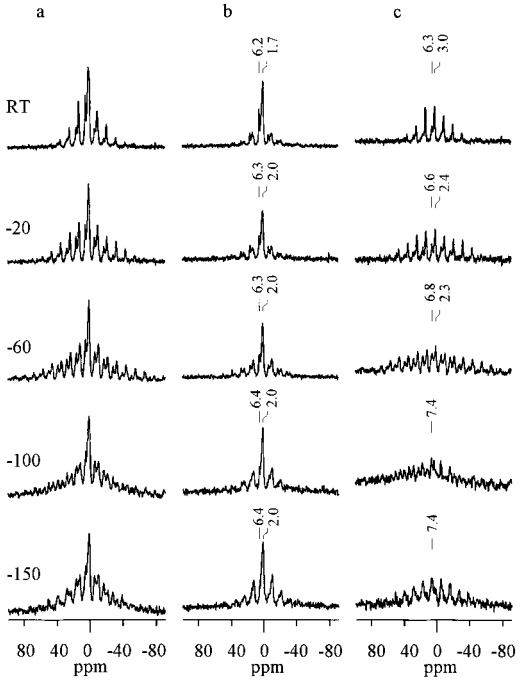

Figure 9. The variable temperature ^{1}H/^{27}Al TRAPDOR NMR spectra of HZSM-5 loaded with 4 O_2/uc acquired (a) with and (b) without ^{27}Al irradiation. Shown in (c) are the difference spectra. Temperatures are marked on the spectra.

^{27}Al irradiation, and (c) the difference spectra are shown in Figure 9. At 25 °C, three resonances are resolved. The two at 6.3 and 2.0 ppm are, as previously assigned, due to water and silanol groups, respectively. The resonance at 3.0 ppm is assigned to the Brønsted acid site, which has shifted by 1 ppm compared to resonance observed for the sample in air. A broader resonance is also observed, underneath the sharp 6.3 ppm peak, with a wider sideband manifold than the 6.3 ppm resonance, and a larger TRAPDOR effect. This resonance is most likely from the second Brønsted acid site. The measured ^{1}H T_1's of the Brønsted acid sites, the water, and the silanols are summarized in Table 2. On lowering the temperature, the sidebands of the silanol-group resonance increase. Meanwhile, the signal due to the Brønsted acid sites gradually shifts to lower frequency and broadens. At −150 °C, all that is left in the difference spectrum is a resonance at 7.0 ppm with large sideband manifolds. To improve the signal-to-noise ratio, the ^{1}H/^{27}Al TRAPDOR NMR experiments at −150 °C were repeated with a recycle delay of 0.01 s (Figure 10), and a similar, apparently simple, difference spectrum was obtained. A TRAPDOR fraction of approximately 90% was observed for the resonance at 7.1 ppm, considerably larger than the value obtained at 25 °C (50%). Again this could result from the reduced motion of the H_2O molecules at lower temperatures. However, when faster MAS spinning rates of 7.0 and 9.0 kHz were used (with a recycle delay of 0.01 s), two sharp resonances at 6.6 and 2.0 ppm were

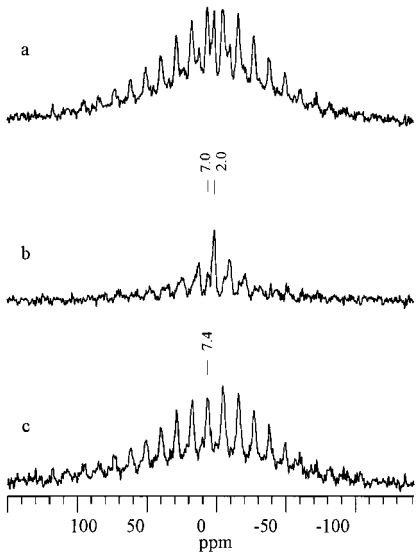

Figure 10. ^{1}H/^{27}Al TRAPDOR NMR spectra of HZSM-5 loaded with 4 O_2/uc acquired (a) with and (b) without ^{27}Al irradiation using a recycle delay of 0.01 s at −150 °C. Shown in (c) is the difference spectrum.

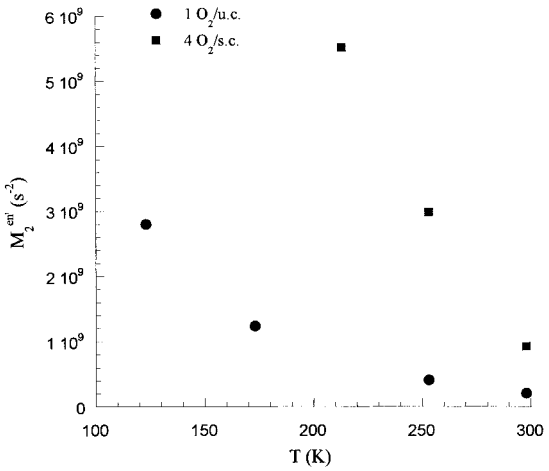

Figure 11. The second moment $M_2^{en'}$ due to the interaction between O_2 and the 4.0 ppm acidic protons in HZSM-5 loaded with (circles) 1 O_2/uc and (squares) 4 O_2/uc as a function of temperature.

observed (not shown). Higher order spinning sidebands, which have a larger line width than either of the two sharp resonances, were also discerned. These broad sidebands are due to a third resonance at approximately −1 ppm. This resonance is from the normal Brønsted acid site, which has shifted significantly at these low temperatures, due to the O_2. At a spinning rate of 4.0 kHz, the broad sidebands of the acidic protons overlap with those due to water at the Lewis acid site, enhancing the apparent TRAPDOR effect of the water resonance.

The second moments of the sideband manifold of the Brønsted acid protons, for the two loaded HZSM-5 samples, were extracted by deconvolution of the difference spectra at each temperature. For the 1 O_2/uc sample, M_2 increased from 7.5×10^8 s^{-2} at 25 °C to 33.4×10^8 s^{-2} at −150 °C. For the 4 O_2/uc sample, a value of 15×10^8 s^{-2} is obtained at 25 °C. Only three data points at above −60 °C are available for this sample due to the broadening out of the signal at lower temperatures. $M_2^{en'}$ was calculated and is plotted as a function of the temperature in Figure 11.

^{29}Si MAS NMR spectra were acquired in N_2 and air at −150 °C for HY and HZSM-5 samples in Kel-F inserts. Because the zeolite samples were dehydrated, broader resonances were

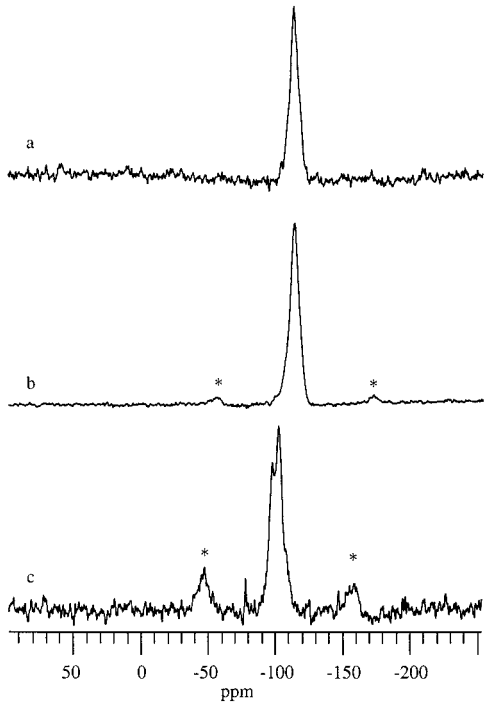

Figure 12. The ^{29}Si MAS NMR spectra of (a) HZSM-5 in N_2, (b) HZSM-5 in air, and (c) HY in air at −150 °C. Spinning speeds of 4.0 kHz were used and the sidebands are denoted with an asterisk.

observed, in comparison to spectra typically observed for hydrated samples, and the signal-to-noise ratio has decreased. The different silicon local environments are no longer so clearly resolved. Figure 12a shows the spectrum of HZSM-5 in N_2, where a peak at −113 ppm is seen, which is due to silicon without any aluminum atoms in the nearest Si/Al coordination sphere. No spinning sidebands are observed. In the presence of air (Figure 12b), first-order sidebands emerge and a second moment of 0.43×10^8 s^{-2} is calculated from the sideband intensities. The first-order spinning sidebands are even more pronounced in the spectrum of HY acquired in air (Figure 12c), resulting in a larger second moment of 1.2×10^8 s^{-2}. The T_1's of ^{29}Si in these two samples are significantly shortened from 7 s, measured for HY in N_2 at −150 °C, to 0.4 s in air.

Discussion

The large sidebands observed in the presence of paramagnets arise primarily from the dipolar coupling between the nuclear (^{1}H) and electronic moments, although bulk magnetic susceptibility effects can also cause significant increases in sidebands.[28,29] The dipolar coupling is a local effect and falls off rapidly as $1/r^3$ where r is the paramagnet−nuclear spin distance. At low loading levels and higher temperatures, rapid isotropic O_2 motion is expected to average this interaction to zero. Little change is observed at room temperature between spectra acquired while spinning in nitrogen and in air, consistent with this. The observation of large spinning sideband envelopes at low temperatures indicates that the O_2 motion can no longer be isotropic, in the time scale of the paramagnet−^{1}H spin interaction. The O_2 must be moving sufficiently slowly, or spending sufficient time complexed to the protons, to result in the increase in sidebands.

The nature of the interaction between O_2 and cations in cation-exchanged zeolites has been studied by many authors, driven primarily by the use of these materials for O_2/N_2 separations.[30,31] The major contribution to the binding energy arises from an electrostatic interaction involving the cation and the quadrupole moment of the O_2 molecule.[31] A quadrupole−H^+ interaction will be operative in the system studied here, and a correlation between proton charge and the size of the interaction with O_2 is expected. O_2 sorption on acidic zeolites has been studied by FT-IR [32] and an absorption due O_2 physisorbed on the Brønsted acid sites in the supercages of HY was observed. The change in the frequency of the O−H stretches of the Brønsted acid sites, on O_2 sorption, was correlated with acidity, a larger shift being observed for O_2 sorption on HZSM-5,[32] which has the higher acid strength.

A much smaller increase in M_2 is observed for the silanol protons at all temperatures, in comparison to the Brønsted acid sites, which is consistent with the lower charge (and acidity) of the silanol protons. The inaccessibility of some of these sites may contribute to the smaller increase in M_2 (this will be discussed in more detail later). The entrance to the sodalite cage in the faujasite structure (through the six-ring window) is approximately 2.6 Å,[33] which is much smaller than the kinetic diameter of the O_2 molecule (3.4 Å).[34] Thus the O_2 molecules do not directly interact with the sodalite cage protons, which is consistent with the smaller increase in M_2 that is observed for protons in the sodalite cages of HY, in comparison to the M_2 values obtained for the supercage protons. Again, O_2 sorption was not observed to effect the IR band of the bridging hydroxyl groups in the sodalite cages,[32] in the earlier FT-IR studies, consistent with this. Similar second moments are observed for the two types of protons in HZSM-5, indicating that they are both accessible to O_2. The second moments obtained at low temperature for HZSM-5 run in air are considerably smaller than those obtained for the supercage protons in HY. This is most likely due to a higher concentration of O_2 in the pores of HY than that in HZSM-5 at constant O_2 partial pressures, the latter containing a much higher Si/Al ratio, and thus fewer proton sites per unit cell.

The large increase in the width of the ^{1}H MAS sideband manifolds and the decrease in the T_1's, as the temperature is lowered, will be caused by two major factors for samples run in air. First, the uptake of O_2 in the pores will increase as the temperature decreases. Second, the time averaged magnetic moment or susceptibility of the oxygen molecule χ will increase at lower temperatures. (For a paramagnet obeying Curie's Law, χ is inversely proportional to the temperature.) A decrease in O_2 motion and/or increase in the time O_2 spends bound to the proton will also occur.

The Hamiltonian for the dipolar coupling between a nucleus I, whose gyromagnetic ratio is γ, and a paramagnet with a time-averaged magnetic moment $\bar{\mu}_e$ is given by[7]

$$H_{en} = \frac{\mu_0}{4\pi}\gamma\bar{\mu}_e \mathbf{D}_{en}\cdot I \tag{3}$$

where the dipolar coupling tensor $\mathbf{D}_{en}$, defined in terms of its matrix elements $D_{\alpha\beta}$, is given by[35]

$$D_{\alpha\beta} = (\delta_{\alpha\beta} - 3e_\alpha e_\beta)/r^3 \tag{4}$$

where r denotes the distance between the nucleus and the electronic moment, δ is the Kronecker delta, and e_α and e_β (α, $\beta = x, y, z$) represent the x, y, or z components of a unit interspin vector in the chosen coordinate system. The time-averaged magnetic moment for a paramagnet can be written as

$$\bar{\mu}_e = \frac{{\mu_B}^2 J(J+1)}{3k_B T}\mathbf{g}\cdot\mathbf{g}\cdot H_0 \quad (5)$$

In the above equation μ_B is the Bohr magneton, k_B is Boltzmann's constant, **g** is the electron **g** tensor, and H_0 is the magnetic field experienced by the paramagnet. J is the total angular momentum number of the paramagnet. In the ground state of an oxygen molecule, two unpaired electrons occupy the two π^* orbitals, giving a total orbital angular momentum number, L, of zero, and a spin angular momentum number, S, of 1. Hence the ground state is ${}^3\Sigma_g^-$ with $J = S = 1$.[36] The second moment arising from this interaction, M_2^{en}, is straightforward to derive, since the Hamiltonian resembles that of the chemical shielding interaction

$$M_2^{en} = \frac{4}{5}\left(\gamma H_0 \frac{\mu_0}{4\pi}\frac{\mathbf{g}^2{\mu_B}^2 J(J+1)}{3k_B T r^3}\right)^2 \quad (6)$$

where an isotropic **g** tensor has been assumed. $(M_2^{en})^{1/2}$ scales linearly with the field, since $\bar{\mu}_e$ is proportional to the field (see (5)). It is then convenient to remove this field dependence by extracting a field-independent anisotropy parameter, $\Delta\sigma^{en}$, which resembles the anisotropy of the chemical shielding[16]

$$\Delta\sigma^{en} = \left(\frac{45}{4}M_2^{en}\right)^{1/2}/\gamma H_0 \quad (7)$$

Here, we have assumed an axially symmetric dipolar-coupling system, which will be the case for coupling to a single isotropic electronic moment. Note that $M_2^{en'}$, the experimentally measured contribution to the total second moment due to the interaction with oxygen, defined in (2), will not necessarily be equal to M_2^{en}, in the presence of a CSA term, M_2^{CSA}. This arises because the CSA and the electron−nuclear dipolar tensors are not necessarily collinear and may also contain values for the principal components that are opposite in sign. Thus, some partial cancelation of these two terms may occur and M_2^{en} and M_2^{CSA} are not strictly additive. Clearly, an error will also be introduced into the value of $\Delta\sigma$, calculated using $M_2^{en'}$ in (7). In the case of two collinear tensors this may be as large as $2\Delta\sigma^{CSA}$.

The situation is more complicated in the case of O_2−zeolite interactions since neither the $O_2-{}^1H$ distance nor the angular terms defined by (4) will be fixed. A time-averaged value of $\mathbf{D}_{en}$, $\bar{D}_{en}$, must be calculated to allow for the oxygen motion. Three principal components D_{xx}, D_{yy}, and D_{zz} may be extracted from $\bar{D}_{en}$ in its principal axis system (i.e., after $\bar{D}_{en}$ has been diagonalized). Clearly, in the limit of very fast O_2 isotropic motion, D_{xx}, D_{yy}, and D_{zz} approach zero.

At least three different processes may be viewed as contributing to $\bar{D}_{en}$ for a hydrogen atom located at the surface of a zeolite pore. One involves the formation of small concentrations of short-lived O_2−Brønsted acid complexes (Si−O(H···O_2)−Al). The complexes are associated with very large values of D_{xx}, D_{yy}, and D_{zz} (due to the small value of r). The second does not involve O_2 directly binding to the protons but arises from a nonzero dipolar interaction with the oxygen molecules within the pores of the zeolite. van der Waals and electrostatic interactions with the walls of the pores will presumably result in slower diffusion and a reduced averaging of the dipolar coupling. The contribution to $\bar{D}_{en}$ from this mechanism should also depend on the shape of the pores of the zeolite. This mechanism should be important even for the protons that are not directly accessible to the oxygen (e.g., the sodalite protons in HY). A third cause of spinning sidebands arises from bulk magnetic susceptibility (BMS) effects; BMS effects will be discussed in more detail later.

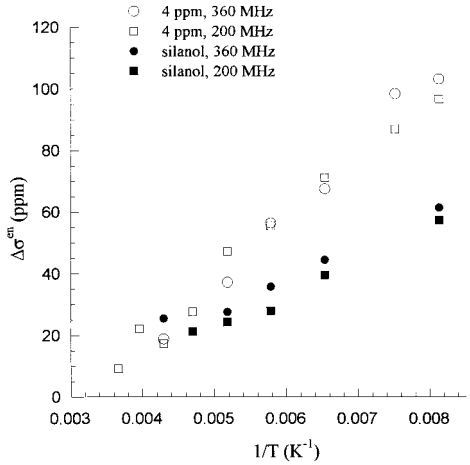

Figure 13. $\Delta\sigma^{en}$ for the Brønsted acid (4 ppm at room temperature, open) and the silanol (solid) protons, for HZSM-5 samples acquired in air, at ^1H frequencies of (circles) 360 MHz and (squares) 200 MHz.

Independent of the mechanism, both increased O_2 accessibility and proton charge (i.e., binding strength) should yield increased values of D_{zz}, via a smaller average value of r. For low loading levels, the dipolar coupling, and thus $\Delta\sigma^{en}$, should also increase linearly with the loading level n_o, which is defined here as the number of O_2 molecules per proton. This should only hold in the regime where $n_o < 1$ and each proton may be assumed to interact with only one oxygen molecule, the other oxygen molecules being very distant.

A plot versus $1/T$ of the experimentally measured increase in the anisotropy of the ^1H resonances due to the interaction with O_2, $\Delta\sigma^{en}$, is shown in Figure 13 for HZSM-5 samples acquired in air, for both the acidic (4 ppm at room temperature) and the silanol protons. Although the relative orientation of the electron−nuclear dipolar coupling and the CSA tensors is unknown, the error in $\Delta\sigma^{en}$ (i.e., the difference between the measured and the true values of $\Delta\sigma^{en}$) is not expected to be large at low temperatures where M_2^{en} is much larger than M_2^{CSA}. The values for $\Delta\sigma^{en}$ for both species, obtained at the same temperature, are essentially independent of field, as predicted, with a deviation of 2−3 ppm from the average value being observed for the measurements acquired at two different field strengths. The ratio of $\Delta\sigma^{en}$ for the acidic protons to $\Delta\sigma^{en}$ for the silanols groups remains fairly constant at 1.7:1 with temperature. Since the loading level of O_2 at a fixed temperature is identical for the two species in the sample sample, the difference in $\Delta\sigma^{en}$ must be dominated by the difference in $\bar{D}_{en}$ (see (4)). Thus the ratio of $\Delta\sigma^{en}$ for two sites may provide one method of discriminating between sites with different H−O_2 binding energies and/or accessibility to O_2 molecules. Surprisingly, the curves of $\Delta\sigma^{en}$ versus $1/T$ for both species are close to being linear, despite the variation in loading level with temperature.

$\Delta\sigma^{en}$ obtained at a ^1H frequency of 360 MHz for samples with a fixed O_2 loading of 1 O_2/uc and 4 O_2/uc, respectively, are plotted versus $1/T$ in Figure 14. As expected, the sample with the higher O_2 loading shows a more rapid increase of $\Delta\sigma^{en}$ with decreasing temperature. The ratio of the slopes for the two curves is 4.0, which is equal to the ratio in oxygen loading levels of the two samples. This is consistent with a linear dependence of $\Delta\sigma^{en}$ on n_o. If the loading of O_2 in the pores remains constant with temperature, a linear curve that goes through the origin is,

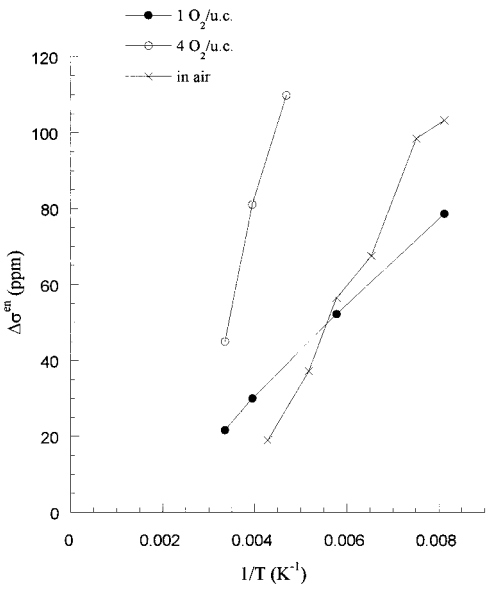

Figure 14. $\Delta\sigma^{en}$ for the Brønsted acid (4 ppm at room temperature) protons in HZSM-5 samples loaded with (solid circles) 1 O_2/uc and (open circles) 4 O_2/uc and for the sample spun in (squares) air.

however, expected (for a Curie paramagnet); this is not observed experimentally, a greater deviation being observed for the higher loading sample. One explanation for this is that there is a certain volume of residual or dead space above the sample in the sealed glass capsule. O_2 will also be present above the sample, in equilibrium with the sorbed O_2, the total amount of O_2 in the capsule being fixed. At lower temperatures more O_2 will be sorbed in the zeolite pores, resulting in a higher loading. Minimizing the dead space and reducing the O_2 loading level should help reduce the change in loading level with temperature of O_2 in the zeolite pores. A more important cause of the deviation may arise from an increase in the binding at low temperatures. This is discussed further below.

The data acquired for the HZSM-5 sample in air at a ^{1}H Larmor frequency of 360 MHz are also shown in Figure 14 for comparison with the data for the 1 O_2/uc sample. To a first approximation, at temperatures above −120 °C, the sample in air has sorbed less than 1 O_2/uc, while below this temperature has sorbed more. The sample run in air, however, will also contain a significant amount of nitrogen in its pores and thus some competitive sorption processes will be occurring in this gas mixture. We can write two expressions to describe this:

$$O_2 + Si{-}O(H){-}Al \longleftrightarrow Si{-}O(H\cdots O_2){-}Al \qquad (8)$$

$$N_2 + Si{-}O(H){-}Al \longleftrightarrow Si{-}O(H\cdots N_2){-}Al \qquad (9)$$

where $Si{-}O(H\cdots N_2){-}Al$ represents an N_2−Brønsted acid site complex. As long as the concentration of $Si{-}O(H\cdots N_2){-}Al$ complexes [$Si{-}O(H\cdots N_2){-}Al$] remains small in comparison to [$Si{-}O(H){-}Al$], then [$Si{-}O(H\cdots O_2){-}Al$] should remain unaffected. This may not be the case at very low temperatures or at high N_2 loading levels. Experiments are currently in progress to examine this in more detail and to determine the effect of varying the N_2/O_2 ratio and loading levels on $M_2^{en'}$. One factor that points to the importance of N_2/O_2 competitive processes is the different ^{1}H shifts observed for the samples run in air and O_2. Larger shifts are always observed for the O_2-loaded samples, even in comparison to samples acquired in air at low temperatures where [O_2] was shown to be greater than 1 O_2/uc. We have previously ascribed these shifts, at least in the ^{133}Cs MAS NMR of CsY, to the formation of discrete complexes.[9] This result suggests that N_2−Brønsted acid site complexation may at least be important in controlling the ^{1}H shifts by reducing [$Si{-}O(H\cdots O_2){-}Al$].

Coupling to a single paramagnet should result in a line shape that resembles that observed for an axially symmetric CSA tensor. This is consistent with the asymmetric line shapes observed in the ^{1}H spectra of the Brønsted acid sites directly accessible to oxygen. The line shapes of the sodalite-cage protons, in contrast, are essentially symmetric, suggesting that additional sources of broadening may be important. Bulk magnetic susceptibility (BMS) broadening has previously been shown to result in increases in sideband manifolds.[37,38] This broadening arises from two different sources: First, when an ellipsoidal particle with nonzero magnetic susceptibility is placed in an originally uniform field, the field in the particle will be uniform, whereas outside it will not. In a powdered material, these field variations will result in nonuniform fields in other particles[28] and consequently inhomogeneous broadening. An additional source of macroscopic field variations occurs for nonspherical particles. For an irregular shape, the induced magnetization varies in direction throughout the particle.[39] For ellipsoids, although the field variations will be uniform throughout each individual particle, the demagnetization factor will depend on its orientation to the field. Inhomogeneous local fields also occur in liquids that are physically inhomogeneous, e.g., suspensions and emulsions,[40−42] and also of particular relevance here, in lung tissue, due to the presence of molecular oxygen in the pores of the lung,[43,44] and result in broadened NMR resonances. Line narrowing will, however, occur on spinning at the magic angle.[40−42,45] Stoll and Majors[37] have demonstrated, for solid-state NMR, that the susceptibility broadening can similarly be removed by sufficiently fast MAS; in the case of large BMS effects, incomplete averaging may occur, resulting in large residual spinning sideband manifolds. Vanderhart et al.[46] and Alla and Lippmaa[47] have shown that the contribution to the residual line widths of the individual peaks within the sideband envelope is then a function of the anisotropic, rather than isotropic, part of the bulk susceptibility of the material. Some broadening of the spinning sidebands in our samples may, therefore, be expected due to BMS effects. These will arise from differences in O_2 concentration in, and outside, the zeolite particles. The BMS effects should, in the absence of proton motion, affect all ^{1}H resonances equally, and thus cannot be the dominant cause of the increase in sidebands of the Brønsted acid sites. They may, however, result in the deviation of the line shapes from those predicted for axially symmetric dipolar-coupling tensors, as has been observed before in other paramagnetic systems.[38] The BMS effect is also negligible at room temperature for samples run in air.

It is difficult to separate the BMS effects from the broadening due to local dipolar coupling interactions involving O_2 and protons that do not directly bind to O_2. These local interactions may also be considered as arising from differences in the magnetic susceptibility of O_2-filled cages, empty cages, and the zeolite framework. To explore the size of this combined interaction, we analyzed the spinning sidebands observed in the ^{29}Si MAS NMR of the same samples, since direct complex formation with the framework silicon atoms, tetrahedrally surrounded by four oxygen atoms, is not expected. Second moments of 0.43×10^8 s^{-2} and 1.25×10^8 s^{-2} for ^{29}Si in

HZSM-5 and HY spun in air at −150 °C, respectively, were estimated. Since the size of the bulk and local dipolar couplings will scale with the gyromagnetic ratios of the nuclei, we can use these numbers to estimate the size of this interaction for ^{1}H. Values for the contribution to $M_2^{en'}$ due to these interactions, of 11×10^8 s^{-2} and 31×10^8 s^{-2} in HZSM-5 and HY, respectively, were obtained. The value for HY is very close to that obtained for the protons in the sodalite cages of HY, confirming the validity of this approach. This result indicates that it will be possible to estimate the contribution to $M_2^{en'}$ due to a combination of bulk effects and nondirectly interacting O_2 molecules, by studying different nuclei or protons in the system that are known to be inaccessible. It will then be possible to subtract this contribution from the values for $M_2^{en'}$ obtained for protons whose location within the porous materials is unknown. The value obtained for HZSM-5 is slightly lower than the value of $M_2^{en'}$ obtained for the silanol groups. This suggests a degree of interaction between at least some of the silanol protons and the O_2. We note, however, that the signal-to-noise of the ^{29}Si NMR spectra of this sample are not good enough to permit any further analyses of this result.

Finally, to explore whether any additional information can be obtained from equations of the form of (3)−(7), and whether the physically observed parameters are close to those predicted from the equations, we have examined the effect of assuming that the O_2 motion and the time-averaging of $\mathbf{D}_{en}$ (radial + angular terms) can all be expressed in terms of an effective or average distance r_{eff}. Any bulk effects will also be included in this effective distance. (6) may then be rewritten as

$$M_2^{en} = \frac{4}{5}\left(\gamma H_0 \frac{\mu_0}{4\pi} \frac{g^2 \mu_B{}^2 J(J+1)}{3k_B T r_{eff}{}^3} n_o\right)^2 \qquad (10)$$

and $\Delta\sigma$ becomes

$$\Delta\sigma^{en} = \frac{\mu_0}{4\pi} \frac{g^2 \mu_B{}^2 J(J+1)}{k_B T r_{eff}{}^3} n_o \qquad (11)$$

From the value of $\Delta\sigma^{en}$ determined for the 1 O_2/uc sample at −150 °C we extracted a r_{eff} of 5.1 ± 0.3 Å. An average distance between Brønsted acid sites in our sample of HZSM-5 is estimated to be approximately 11 Å. Thus, these distances are of the order of half the average H−H distance and are of the expected order of magnitude. Further analyses and experiments are currently in progress to extract r_{eff} for a range of different acidic zeolites to determine some of the factors that control this number (e.g., acidity and pore shape) and to explore whether any more detailed structural information may be obtained from this approach. Clearly, to derive a more accurate model, further calculations, which may include molecular dynamics calculations (to extract, for example, radial distribution values), will be required.

Conclusions

Large changes in the width of the spinning sidebands envelopes of sites that are directly accessible to O_2 are observed in the variable temperature ^{1}H MAS NMR of O_2-sorbed zeolites. These results suggest novel methods for probing O_2 binding in zeolites and molecular sieves and for probing accessibility of pores to small gases in a wide range of porous materials. In addition, the experiments can readily be extended to study competitive binding between O_2 and other gases. Experiments are currently in progress to apply the method to some of these systems. Finally, the results have implications for studying other materials at low temperatures in unsealed MAS rotors: O_2 condensation or sorption may occur, altering T_1's, shifts, and spinning sideband manifolds.

Acknowledgment. Support from the NSF is acknowledged (Grants DMR 9458017 and CHE 9405436). Helpful discussions with Dr. P. McDaniel are gratefully acknowledged.

References and Notes

(1) Dobson, C. M.; Levine, B. A. *New Techniques in Biophysics and Cell Biology*; Wiley-Interscience: New York, 1976.
(2) Hinckley, C. *J. Am. Chem. Soc.* **1969**, *91*, 5160.
(3) Inagaki, F.; Miyazawa, T. *Prog. NMR Spectrosc.* **1981**, *14*, 67.
(4) Lee, Y. J.; Wang, F.; Grey, C. P. *J. Am. Chem. Soc.* **1998**, *120*, 12601.
(5) Liu, K.; Ryan, D.; Nakanishi, K.; McDermott, A. *J. Am. Chem. Soc.* **1995**, *117*, 6897.
(6) Grey, C. P.; Dobson, C. M.; Cheetham, A. K.; Jakeman, R. J. B. *J. Am. Chem. Soc.* **1989**, *111*, 505.
(7) Nayeem, A.; Yesinowski, J. P. *J. Chem. Phys.* **1988**, *89*, 4600.
(8) Klinowski, J.; Carpenter, T. A.; Thomas, J. M. *J. Chem. Soc., Chem. Commun.* **1986**, 956.
(9) Liu, H.; Kao, H.-M.; Grey, C. P. In *Proceedings of the 12th International Zeolite Conference*; Treacy, M. M. J., Marcus, B. K., Bisher, M. E., Higgins, J. B., Eds.; Material Research Society: Baltimore, MD, 1998; Vol. 4, p 2317.
(10) Plévert, J.; Ménorval, L. C. d.; Renzo, F. D.; Fajula, F. *J. Phys. Chem. B* **1998**, *102*, 3412.
(11) Feuerstein, M.; Lobo, R. F. *Chem. Commun.* **1998**, *016*, 1647.
(12) Zscherpel, D.; Brunner, E.; Koch, M. *Z. Phys. Chem.* **1995**, *190*, 123.
(13) Norby, P.; Poshni, F. I.; Gualtieri, A. F.; Hanson, J. H.; Grey, C. P. *J. Phys. Chem. B* **1998**, *102*, 839.
(14) Grey, C. P.; Vega, A. J. *J. Am. Chem. Soc.* **1995**, *117*, 8232.
(15) Grey, C. P.; Veeman, W. S.; Vega, A. J. *J. Chem. Phys.* **1993**, *98*, 7711.
(16) Maricq, M. M.; Waugh, J. S. *J. Chem. Phys.* **1979**, *70*, 3300.
(17) Fenzke, D.; Hunger, M.; Pfeifer, H. *J. Magn. Reson.* **1991**, *95*, 477.
(18) Hunger, M.; Anderson, M. W.; Ojo, A.; Pfeifer, H. *Micorporous Mater.* **1993**, *1*, 17.
(19) Jacobs, W. P. J. H.; de Haan, J. W.; van der Ven, L. J. M.; van Santen, R. A. *J. Phys. Chem.* **1993**, *97*, 10394.
(20) Freude, D.; Klinowski, J.; Hamdan, H. *Chem. Phys. Lett.* **1988**, *149*, 355.
(21) Kenaston, N. P.; Bell, A. T.; Reimer, J. A. *J. Phys. Chem.* **1994**, *98*, 894.
(22) Brunner, E.; Beck, K.; Koch, M.; Pfeifer, H.; Staudte, B.; Zscherpel, D. *Stud. Surf. Sci. Catal.* **1994**, *84*, 357.
(23) Beck, L. W.; White, J. L.; Haw, J. M. *J. Am. Chem. Soc.* **1994**, *116*, 9657.
(24) Freude, D. *Chem. Phys. Lett.* **1995**, *235*, 69.
(25) Sarv, P.; Tuherm, T.; Lippmaa, E.; Keskien, K.; Root, A. *J. Phys. Chem.* **1995**, *99*, 13763.
(26) Hunger, M.; Freude, D.; Pfeifer, H. *J. Chem. Soc., Faraday Trans.* **1991**, *87*, 857.
(27) Deng, F.; Yue, Y.; Ye, C. *Solid State Nucl. Magn. Reson.* **1998**, *10*, 151.
(28) Drain, L. E. *Proc. Phys. Soc.* **1962**, *80*, 1389.
(29) Grey, C. P. Ph.D. Thesis, University of Oxford, 1991.
(30) Coe, C. G.; Kirner, J. F.; Pierantozzi, R.; White, T. R. *U.S. Patent*, **1992**, *5*, 813.
(31) Papai, I.; Guorsot, A.; Fajula, F.; Plee, D.; Weber, J. *J. Phys. Chem.* **1995**, *99*, 12925.
(32) Wakabayashi, F.; Kondo, J. N.; Domen, K.; Hirose, C. *Microporous Mater.* **1997**, *8*, 29.
(33) Smart, L.; Moore, E. *Solid State Chemistry*: *An Introduction*, 1st ed.; Chapman & Hall: London, 1992; p 190.
(34) Breck, D. W. *Zeolite Molecular Sieves: Structure, Chemistry and Use*; John Wiley & Sons: New York, 1974; p 677.
(35) Mehring, M. *Principles of High-Resolution NMR in Solids*, 2nd ed.; Springer-Verlag: Berlin, 1983.
(36) Ardon, M. *Oxygen: Elementary Forms and Hydrogen Peroxide*; W. A. Benjamin, Inc.: New York, 1965; p 32.
(37) Stoll, M. E.; Majors, T. J. *Phys. Rev. B* **1981**, *24*, 2859.
(38) Grey, C. P.; Dobson, C. M.; A. K. Cheetham, A. K. *J. Magn. Reson.* **1992**, *98*, 414.
(39) Osborn, J. A. *Phys. Rev.* **1945**, *67*, 351.

(40) Doskocilová, D.; Schneider, B. *Chem. Phys. Lett* **1970**, *6*, 381.
(41) Doskocilová, D.; Schneider, B. *Macromolecules* **1972**, *5*, 125.
(42) Doskocilová, D.; Tao, D. D.; Schneider, B. *Czech J. Phys. B* **1975**, *25*, 202.
(43) Case, T. A.; Durney, C. H.; Ailion, D. C.; Cutillo, A. G.; Morris, A. H. *J. Magn. Reson.* **1987**, *73*, 304.
(44) Durney, C. H.; Bertolina, J.; Ailion, D. C.; Christiman, R.; Cutillo, A. G.; Morris, A. H.; Hashemi, S. *J. Magn. Reson.* **1989**, *85*, 544.
(45) Garroway, A. N. *J. Magn. Reson.* **1982**, *49*, 168.
(46) Vanderhart, D. L.; Earl, W. L.; Garroway, A. N. *J. Magn. Reson.* **1981**, *44*, 361.
(47) Alla, M.; Lippmaa, E. *Chem. Phys. Lett.* **1982**, *87*, 30.